

**406 Retrievals of Warm-Rain Microphysics Using X-Band Polarimetric Radar Data**Matthew R. Kumjian<sup>1\*</sup>, Alexander Ryzhkov<sup>1</sup>, Silke Trömel<sup>2</sup>, Malte Diederich<sup>2</sup>, Kai Mühlbauer<sup>2</sup>, and Clemens Simmer<sup>2</sup>1. *Cooperative Institute for Mesoscale Meteorological Studies, University of Oklahoma, Norman, OK, USA*2. *Meteorological Institute of the University of Bonn, Bonn, Germany***1. Introduction.**

Precipitation growth via the “warm rain processes” does not involve ice particles, as the name implies. Instead, cloud droplets grow by condensation until they become sufficiently large as to sediment relative to the other droplets. Once such sedimentation occurs, droplet growth quickly continues by accretion of other cloud droplets different in size (and thus fall speed), whereupon the collecting droplet rapidly grows in size to a raindrop. Apparently, only 1 droplet in  $10^6$  must attain sufficiently large size to initiate the production of precipitation (e.g., Rogers and Yau 1989; Pruppacher and Klett 1997).

As the precipitation particles fall to the ground, the evolution of the DSD beneath cloud base is governed by four main processes: growth of large drops (and subsequent depletion of small drops) by coalescence, depletion of large drops (and increase in concentration of smaller drops) by collisional breakup, size sorting of drops, and a decrease of drop sizes across the spectrum (and depletion of the smallest drops) by evaporation. The latter is not as important in cases of heavy rain. The equation governing the evolution of number density  $n$  in time by the collisional processes can be written as (Gillespie and List 1978; Brown 1995, among others):

$$\begin{aligned} \frac{\partial n(m, t)}{\partial t} &= \int_{m/2}^{\infty} \int_0^{\mu} n(\mu, t) n(\mu_1, t) f(\mu, \mu_1) [1 \\ &\quad - E(\mu, \mu_1)] Q(m; \mu, \mu_1) d\mu_1 d\mu \\ &\quad - \int_0^{m/2} n(m, t) n(\mu_1, t) f(m, \mu_1) [1 - E(m, \mu_1)] d\mu_1 \\ &\quad + \int_0^{\infty} n(\mu, t) n(m - \mu, t) f(\mu, m - \mu) E(\mu, m - \mu) d\mu \\ &\quad - \int_0^{\infty} n(m, t) n(\mu, t) f(\mu, m) E(\mu, m) d\mu \end{aligned} \quad (1)$$

In eqn. (1), the first two terms on the RHS represent drop breakup, and the latter two terms represent drop coalescence. Here,  $E(\mu, \mu_1)$  is the coalescence efficiency for drops of masses  $\mu$  and  $\mu_1$ ,  $Q(m; \mu, \mu_1)\Delta m$  is the average number of drop fragments with mass  $m$  to  $m + \Delta m$  produced by collision and subsequent breakup of drops with masses  $\mu$  and  $\mu_1$ , and  $f(\mu, \mu_1)$  is the collision kernel.

The collision kernel is given by

$$f(\mu, \mu_1) = \pi (r_{\mu} + r_{\mu_1})^2 E_{col}(\mu, \mu_1) |V_{\mu_1} - V_{\mu}|, \quad (2)$$

where  $r_{\mu}$  is the radius of a drop with mass  $\mu$ ,  $E_{col}$  is the collision efficiency of drops with masses  $\mu$  and  $\mu_1$ , and  $V_{\mu}$  is the falling velocity of a drop with mass  $\mu$ . Obviously, the equation is rather complex. As such, there have been many studies of this equation, methods for solving it, and its parameterizations (Low and List 1982a,b; Brown

---

\*Corresponding author: 120 David L. Boren Blvd., National Weather Center Suite 4900, Norman, Oklahoma, USA 73071.

Email: matthew.kumjian@noaa.gov

1986, 1987, 1993, 1994; List et al. 1987; List and McFarquhar 1990). In contrast, there have been relatively few studies of these processes in nature, such as remote sensing-based retrievals of changes in the DSD owing to these processes. Dual-polarization radar in particular is well-suited for such a study, as the polarimetric radar variables are sensitive to changes in the overall shape of the rain DSD, especially the large-drop end of the size spectrum. This sensitivity is particularly pronounced at shorter radar wavelengths (C and X bands).

This study investigates vertical profiles of the polarimetric radar variables in warm-rain precipitation, in situations when coalescence growth evidently is a dominant process. Based on these data, DSD parameters are retrieved to explore the vertical evolution of the DSD in ongoing coalescence.

## 2. Coalescence: a *Gedankenexperiment*.

Consider two identical drops with mass  $m_1$  and diameter  $D_1 = (6m_1/\pi\rho_w)^{1/3}$ , where  $\rho_w$  is the density of liquid water. A collection of  $N_1$  of these drops would result in a radar reflectivity factor (in the Rayleigh approximation)  $Z_1 = N_1 D_1^6$ . Consider now that these two drops collide and coalesce to form one larger drop of mass  $m_2 = 2m_1$ . It follows that the diameter  $D_2$  of the new big drop is  $D_2 = 2^{1/3} D_1$ , and the concentration of the big drop  $N_2 = 0.5 N_1$ . Thus, we can calculate the Rayleigh radar reflectivity factor of the new big drop:

$$Z_2 = N_2 D_2^6 = 0.5 N_1 (2^{1/3} D_1)^6 = 2 N_1 D_1^6 = 2 Z_1$$

In other words, the new reflectivity factor is 3 dBZ larger than before the two drops coalesce. We can perform the same analysis for  $K_{DP}$ , which is dependent on drop diameters as  $D^4$  to  $D^6$ , depending on the rainfall rate. It is clear that for

the smaller dependence on diameter, the change in  $K_{DP}$  is less. (If we assume, for the sake of argument, that  $K_{DP} \propto D^5$ , then  $K_{DP2} \approx 1.6 K_{DP1}$ ). Thus, we can conclude that coalescence effects  $K_{DP}$  (in general) less than  $Z$ . Because drop oblateness monotonically increases with increasing drop size, it follows that coalescence of two smaller drops tends to increase  $Z_{DR}$  (as a result of the increased oblateness and size of the new big drop).

Using the simple power-law relation of Atlas and Ulbrich (1977) for the relation between drop size and terminal velocity ( $v \propto D^{0.67}$ ), the same analysis reveals that rainfall rate  $R$  increases for coalescence, owing to the larger drop sizes:

$$R_2 = N_2 D_2^3 v_2 \sim N_2 D_2^{3.67} = 0.5 N_1 (2^{1/3} D_1)^{3.67} \approx 1.167 R_1$$

It is clear that only those quantities proportional to  $D^x$  for  $x > 3.0$  are *increased* by the process of coalescence, which includes Rayleigh reflectivity factor  $Z$ ,  $K_{DP}$ ,  $Z_{DR}$ , and rainfall rate. Liquid water content  $M$  is proportional to the third moment of the DSD and thus is not changed during pure coalescence. In other words, the total amount of liquid water mass is conserved during coalescence; it is simply redistributed among the drop sizes. That  $M$  is conserved during pure coalescence will be a fundamental assumption of the microphysical retrievals in the following sections.

## 3. Data.

Data from the Bonn X-band Polarimetric (BOXPOL) radar in Bonn, Germany are presented here. Radar specifications for BOXPOL are presented in Table 1. Genuine RHIs were collected with  $0.1^\circ$  spacing in elevation, affording high spatial resolution. The precipitation event occurred on 22 June 2011, in which several warm-rain storms were observed (e.g., Figure 1).

Ten vertical profiles are extracted from this RHI between 13 and 14 km range. The median of these profiles is then constructed (Figs. 2-3). The data reveal a distinct, well-pronounced increase in both  $Z_H$  and  $Z_{DR}$  towards the ground, indicative of increasingly larger drops present closer to the ground. Note that this differs from the signature of differential sedimentation, where  $Z_H$  decreases as  $Z_{DR}$  increases (Kumjian and Ryzhkov 2012). Differential sedimentation is seen in the

developing cell at 11 km range. Instead, the profiles in Figures 2-3 provide a clear indication of raindrop growth (and the radar signal) being dominated by coalescence. Collisional breakup (which tends to decrease  $Z_{DR}$ ) is undoubtedly occurring, but it is not enough to balance the overall contribution of coalescence to the radar signal. Note that the data below about 600 m in height are contaminated by ground clutter and have been censored from Figures 2 and 3.

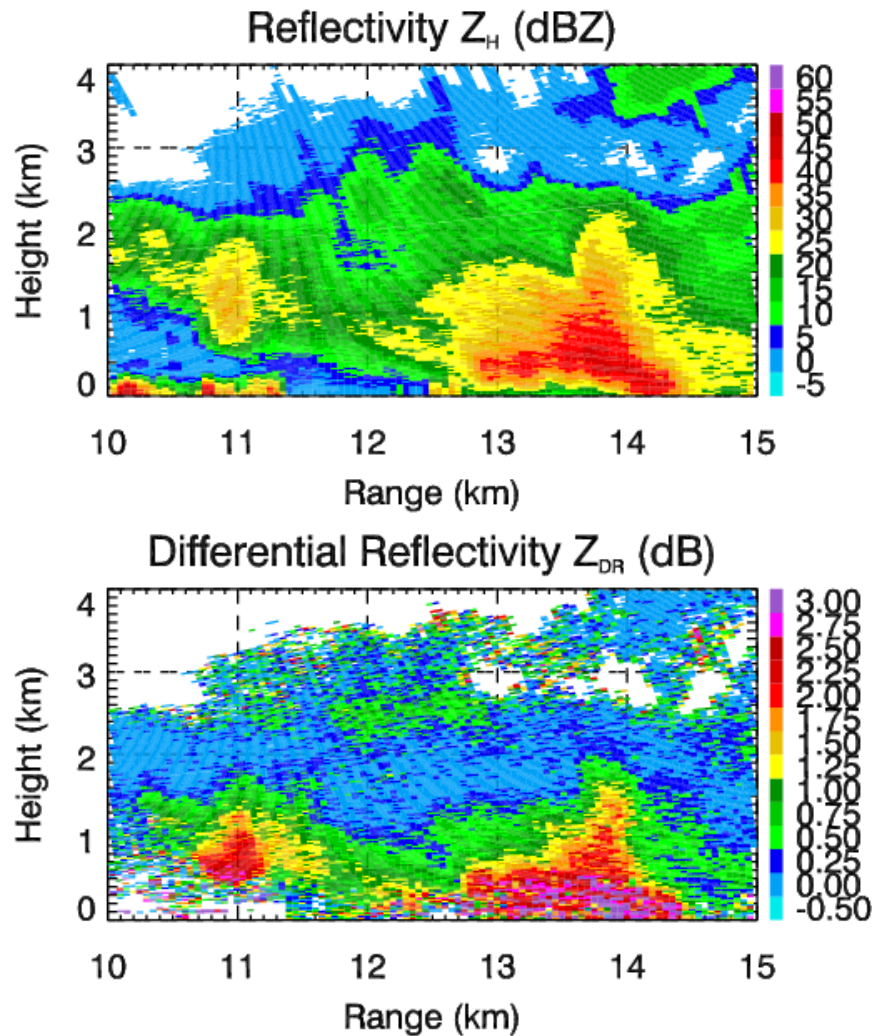


Fig. 1: Genuine RHI scan collected with BOXPOL on 22 June 2011 at 1454 UTC, along the  $309.5^\circ$  azimuth. Polarimetric radar variables shown are (top)  $Z_H$ , and (bottom)  $Z_{DR}$ . The cell of interest is located between 13 and 14 km range.

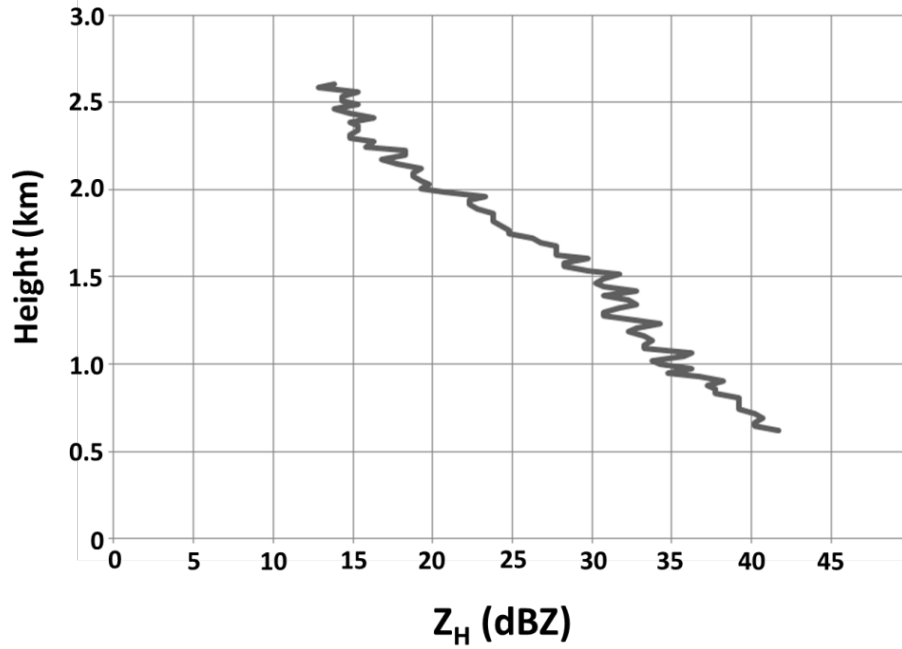


Fig. 2: Median vertical profile of  $Z_H$  through the storm in Figure 1, constructed from 10 extracted vertical profiles at ranges 13 – 14 km.

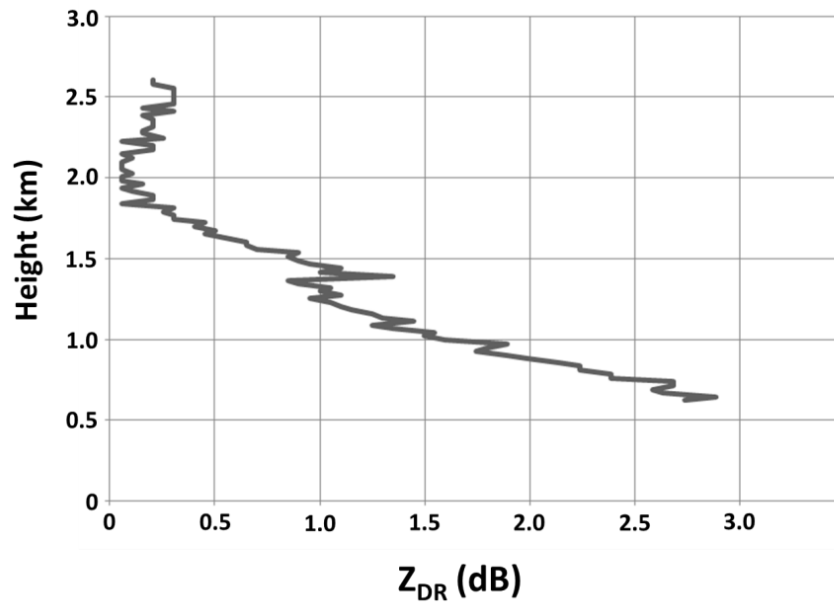


Fig. 3: Median vertical profile of  $Z_{DR}$  through the storm in Figure 1, constructed from 10 extracted vertical profiles at ranges 13 – 14 km.

<b>BOXPOL Radar Characteristics</b>	
<b>Wavelength</b>	<b>3.21 cm (X band)</b>
<b>Antenna beamwidth (-3 dB)</b>	<b>1.06°</b>
<b>Peak Power</b>	<b>200 kW</b>
<b>Range resolution</b>	<b>50 m (50 km max. range)</b>
<b>Scanning strategy</b>	<b>RHI; 0.1° spacing in elevation; along the 309.5° azimuth</b>

*Table 1: Characteristics of the BOXPOL radar*

#### 4. Microphysical Retrievals: Methods.

Dual-polarization radar observations have the unique capability of being used to retrieve information about the rain DSD shape (e.g., Zhang et al. 2001; Brandes et al. 2002, 2004). For this study, calculations of the dual-polarization radar variables for a wide range of DSDs found in nature modeled by the constrained-gamma relation (e.g., Zhang et al. 2001, 2003)

$$N(D) = N_0 D^\mu \exp(-\Lambda D) \quad (3)$$

were performed. The constrained gamma DSD is constrained by an assumed relation between shape parameter  $\mu$  and slope parameter  $\Lambda$ , which has been observed in natural DSDs (e.g., Cao et al. 2008):

$$\mu = -0.0201\Lambda^2 + 0.902\Lambda - 1.718, \quad (4)$$

where here  $\Lambda$  is in  $\text{mm}^{-1}$ . The constrained-gamma relation is convenient in that there exists a relation between the DSD slope parameter  $\Lambda$  and  $Z_{DR}$  (Fig. 4). The T-matrix method (Mischenko

2000) was used to compute the complex scattering amplitudes of raindrops at X band with a temperature of 15 °C, from which the polarimetric variables were computed following Ryzhkov (2001) and Ryzhkov et al. (2011). The  $\mu$ - $\Lambda$  relation from Cao et al. (2008) is used to determine the  $Z_{DR}$  for a given slope parameter  $\Lambda$ . Though some controversy exists about the physical nature of this relation (e.g., see Zhang et al. 2003; Seifert 2005; Moisseev and Chandrasekar 2007), it is clear from Figure 4 that it lies within the natural range of values. The observed  $Z_{DR}$  profile is compared to the  $\Lambda$ - $Z_{DR}$  relation to determine the best match for  $\Lambda$ . Then, the retrieved profile of  $\Lambda$  is used with eqn. (4) to retrieve the vertical profile of  $\mu$  (Fig. 5). A vertical profile of  $Z_{DR}$  is computed based on the retrieved  $\Lambda$  and  $\mu$  values (remember that  $Z_{DR}$  is independent of concentration and thus does not depend on  $N_0$ ). Obviously, one should expect this retrieved  $Z_{DR}$  to agree very well with the observed profile.

At the bottom of the profile, total liquid water content  $M$ ,

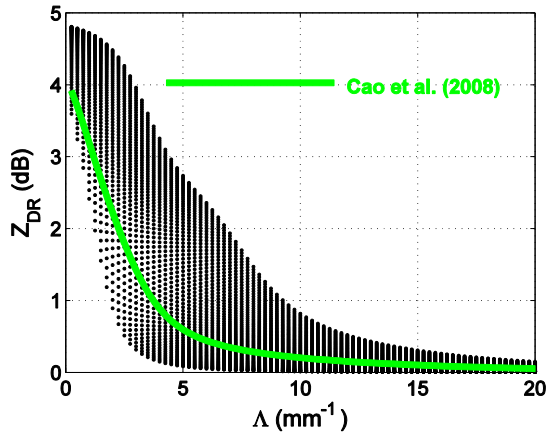


Fig. 4: Scatter of the range of  $\Lambda$ - $Z_{DR}$  points observed in nature (black points), overlaid with the  $Z_{DR}$  from the Cao et al. (2008) relation (green). Calculations made at X band, for raindrops with temperature = 15 °C.

$$M = \frac{\pi}{6} \rho_w \int_0^{\infty} N(D) D^3 dD \quad (5)$$

is determined (rather subjectively) based on what provides best match of the observed profiles of the polarimetric radar variables. From this height, the flux of liquid water mass content  $M$  is assumed to remain constant with height

$$Mv = M_{ref}v_{ref} = \text{constant}. \quad (6)$$

In other words, we assume that no water mass is lost owing to evaporation; rather, mass is simply shifted from size bin to size bin by coalescence, and is affected by the change in fallspeed with height owing to changes in air density. Air density is determined from the 12 UTC sounding on 22 June 2011 from Essen, Germany (Fig. 6), located roughly 90 km to the north-northwest of Bonn. Using  $M$ ,  $\mu$ , and  $\Lambda$  at each height, intercept parameter  $N_0$  is determined by solving (5):

$$N_0 = \frac{6M\Lambda^{4+\mu}}{\pi\rho_w\Gamma(4+\mu)}, \quad (7)$$

where  $\Gamma$  is the gamma function. The retrieved DSD at each level is then determined by equation (3). Note that  $Z_H$  is not used to determine the DSD parameters; rather, the  $Z_H$  calculated from the retrieved DSD will be compared to observations as a test of the methods and assumptions.

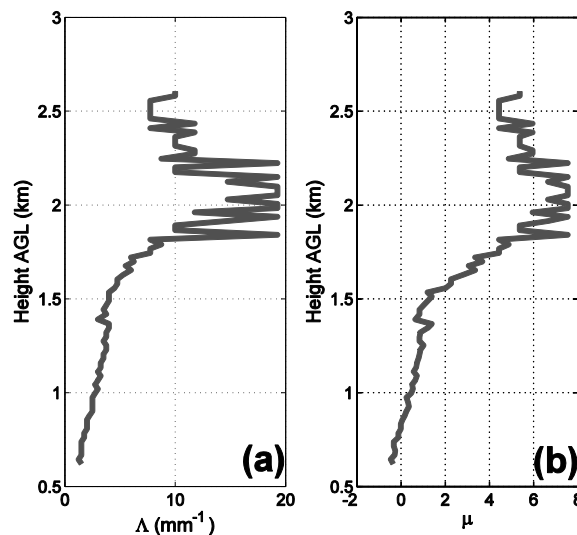


Fig. 5: Vertical profiles of slope parameter  $\Lambda$  (left) and shape parameter  $\mu$  (right) retrieved from polarimetric radar measurements.

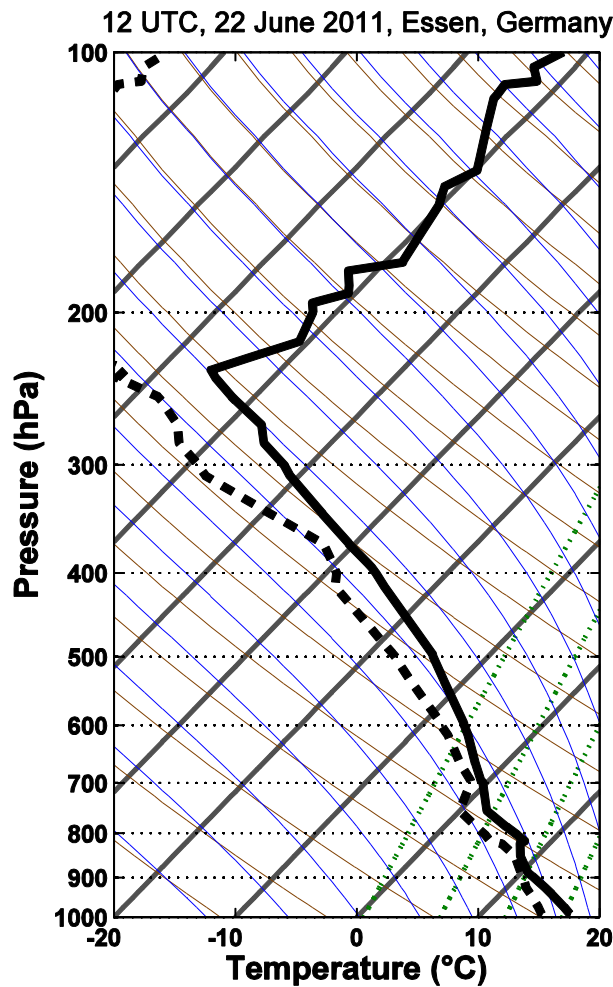


Fig. 6: Observed sounding from Essen, Germany, on 22 June 2011 at 12 UTC.

### 5. Microphysical Retrievals: Results.

The vertical profiles of polarimetric radar variables  $Z_H$  and  $Z_{DR}$  are calculated from the retrieved DSD at each level. Figure 7 compares the retrieved  $Z_{DR}$  profile to the observed  $Z_{DR}$  profile. As expected, there is very good agreement over all height levels. This is because the  $Z_{DR}$ - $\Lambda$  relation was used as an input to the retrieval. Figure 8 shows the retrieved vertical profile of  $Z_H$  compared to the observations. Recall that  $Z_H$  is under the constraint that the flux of the mass water content is conserved at each level. The surprisingly good

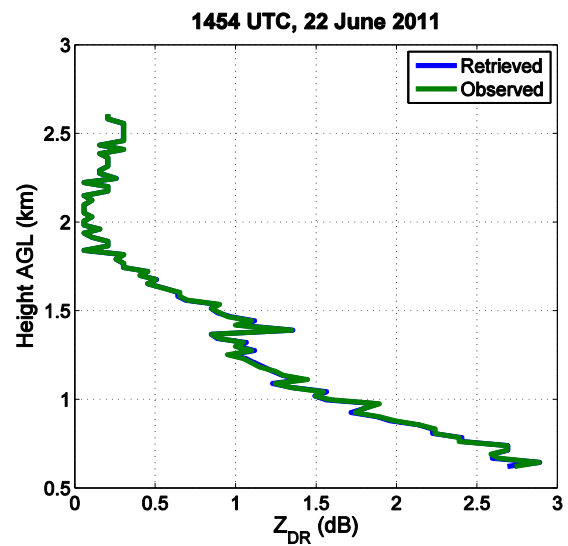


Fig. 7: Retrieved  $Z_{DR}$  (blue curve) and the observed  $Z_{DR}$  (green curve) profiles as a function of height.

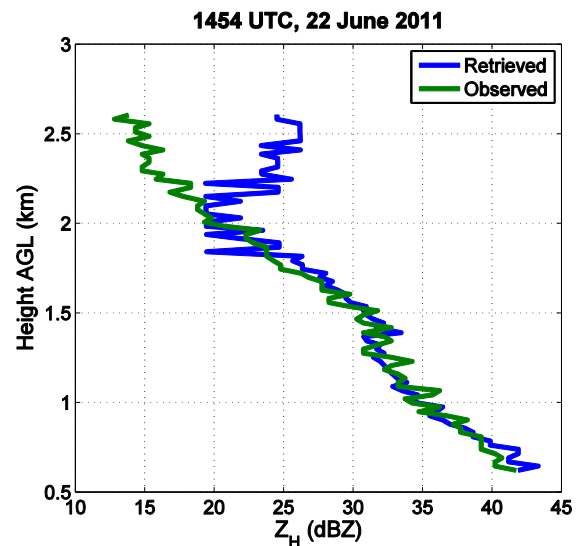


Fig. 8: As in Figure 7, but the retrieved (blue) and observed (green)  $Z_H$  profiles are shown.

agreement below about 2 km indicates that this assumption is likely valid; in other words, coalescence is the dominant process below this height. Indeed, relative errors (Fig. 9) below 2 km AGL are within  $\pm 10\%$ . The disagreement between retrieved and observed  $Z_H$  above about 2 km is also informative. It demonstrates that the assumption of constant  $M$  flux in this height

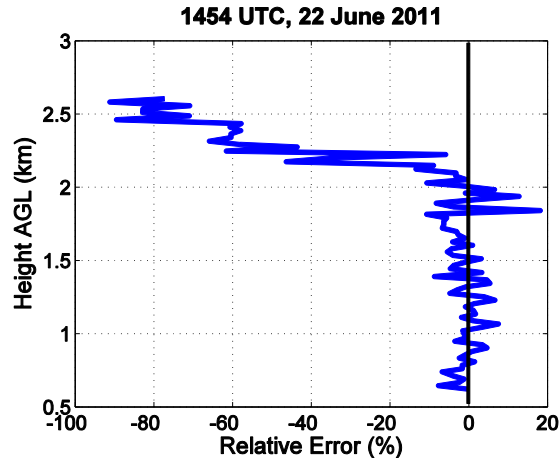


Fig. 9: Relative error (%) of the retrieved  $Z_H$  profile for 1454 UTC on 22 June 2011.

interval is not valid. We can infer this because the  $Z_{DR}$  profiles match very well, implying that the overall shape of the DSD ( $\mu$  and  $\Lambda$ ) are rather close to reality. In other words, there is likely a change in  $M$  with height above about 2 km. Because the retrieved profile has larger values of  $Z_H$  above 2 km than the observed profile, but matches rather well below 2 km, one can infer that  $M$  is being *generated* or added at levels above 2 km, owing to activation of more drops (e.g., within an updraft) or accretion of cloud water droplets.

The retrieved DSD at each level (Figure 10) reveal the evolution of DSDs undergoing pure coalescence. It is important to emphasize that we do not attempt to perfectly retrieve the actual DSD; rather, the retrieval provides a *plausible* look at the evolution of the DSD in height affected by pure coalescence. Indeed, disagreement between the retrieved profiles and the observations is also instructive, as illustrated above. Moving towards the ground (colors in Figure 10 transition from black to blue to red) the concentration of smaller drops ( $< 1.5$  mm) decreases substantially as the concentration of large drops increases and the DSD broadens. Note that this effect is retrieved solely from our

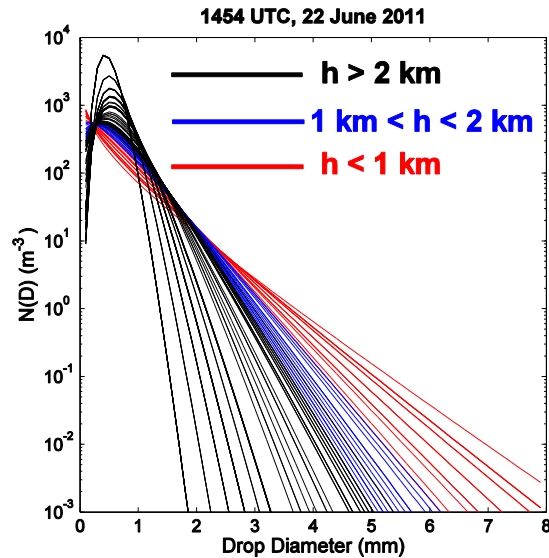


Figure 10: Retrieved DSD at each height level, with each color indicating a certain depth. As expected with coalescence growth, the initially narrow DSD broadens and acquires a shallower slope, indicative of an increase in concentration of large drops and a decrease in concentration of small drops (sizes  $< 2$  mm).

assumptions and polarimetric data; no physical parameterization of coalescence has been implemented.

These retrieved DSDs can be used to compute the other polarimetric radar variables  $K_{DP}$  and  $\rho_{hv}$  (Fig. 11). Note the increase in  $K_{DP}$  towards the ground; similar to  $Z_H$ , this implies that the increase in particle size overcomes the decrease in particle concentration. This result also agrees well with the *gedankenexperiment* described earlier: if converted to logarithmic units, the increase in  $K_{DP}$  is about 12 dBZ, which is less than the increase in  $Z_H$  (closer to 20 dBZ). The decrease in the retrieved  $\rho_{hv}$ , though small in magnitude, is consistent with the broadening of the DSD depicted by Figure 10.

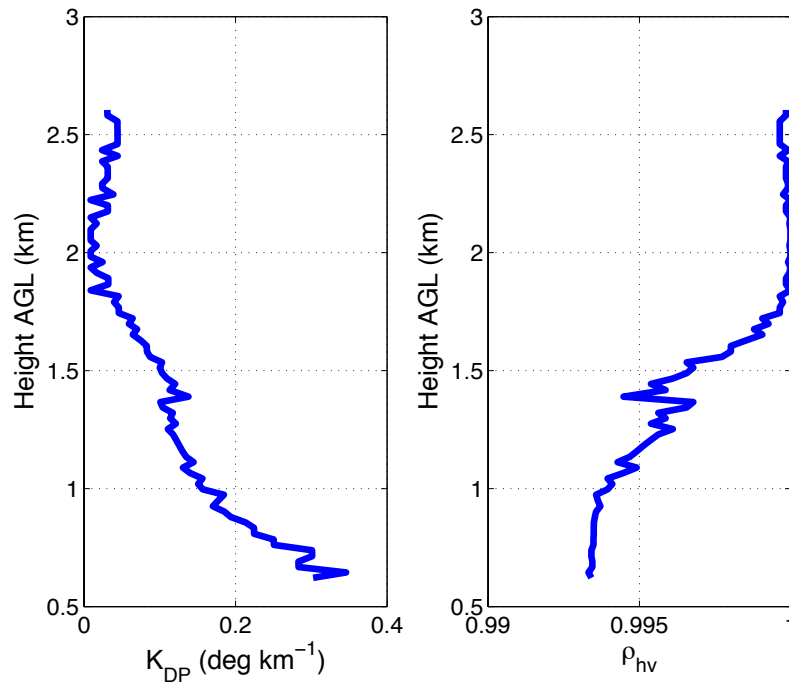


Fig. 11: Retrieved profiles of  $K_{DP}$  (left panel) and  $\rho_{hv}$  (right panel) from 22 June 2011, 1454 UTC.

### 6. Size Sorting.

In addition to coalescence, cases of size sorting are clear in the observed data. For example, the cell centered at about 11 km in range in Figure 1 displays a sharp increase in  $Z_{DR}$  towards the ground, collocated with a decrease in  $Z_H$ . Though evaporation similarly causes an increase in  $Z_{DR}$  and decrease in  $Z_H$  (e.g., Kumjian and Ryzhkov 2010), the magnitude of the  $Z_{DR}$  increase implies size sorting is the dominant process in this case.

Earlier in the day on 22 June, another case of transient differential sedimentation was captured with the BOXPOL radar. A scatterplot of the observed  $Z_H$  and  $Z_{DR}$  (Figure 12) reveals a striking inverse correlation, remarkably different from what is expected in rain. Such an inverse correlation is a tell-tale sign of raindrop size sorting (e.g., Kumjian and Ryzhkov 2012). Though

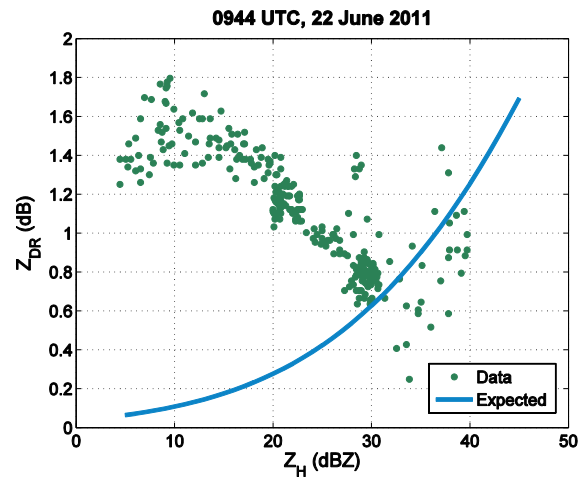


Fig. 12:  $Z_H$ - $Z_{DR}$  scatter of data from 0944 UTC on 22 June 2011 (green points) compared to the "expected"  $Z_H$ - $Z_{DR}$  relation of Cao et al. (2008).

such differential sedimentation is transient, size sorting can be maintained in the presence of updrafts or vertical wind shear. Again, such a case was captured with BOXPOL (Fig. 13a,b). Although

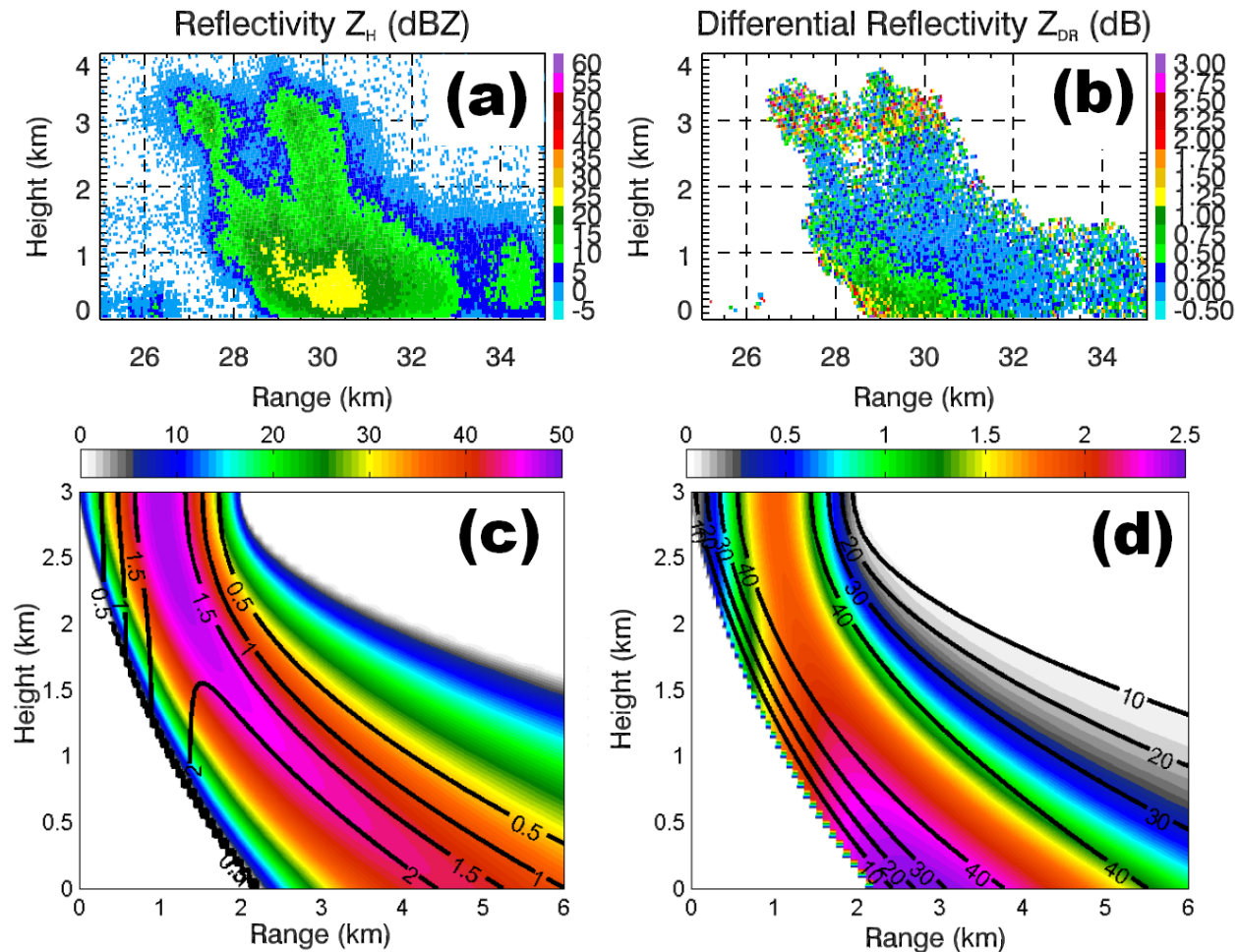


Fig. 13: Comparison of observed and modeled polarimetric variables of a rainshaft encountering vertical wind shear. (a) Observed  $Z_H$ , and (b) observed  $Z_{DR}$  from 22 June 2011, at 0404 UTC, from BOXPOL radar. (c) Modeled  $Z_H$ , with contours of  $Z_{DR}$  overlaid, and (d) modeled  $Z_{DR}$ , with contours of  $Z_H$  overlaid. Adapted from Kumjian and Ryzhkov (2012).

a melting layer “bright band” is evident, implying ice particles are present, the size sorting effect is most pronounced in the pure rain part of the echo. The enhancement of  $Z_{DR}$  found at the leading edge of the cell, along a gradient in  $Z_H$  closely resembles the idealized modeling results (Fig. 13c,d) of Kumjian and Ryzhkov (2012).

## 7. Discussion and Conclusions.

The impact of the main warm-rain microphysical processes on the polarimetric radar variables is summarized pictorially in Figure 14.

Whereas one radar variable alone cannot provide enough information to differentiate between the dominant ongoing process, polarimetry greatly reduces this ambiguity. Each microphysical process has its own “fingerprint” in the polarimetric data, which can be exploited for microphysical retrievals and model microphysics validation studies.

A method for retrieving microphysical information was presented. In the case of coalescence, fundamental physical assumptions lead to testable predictions about the changes in

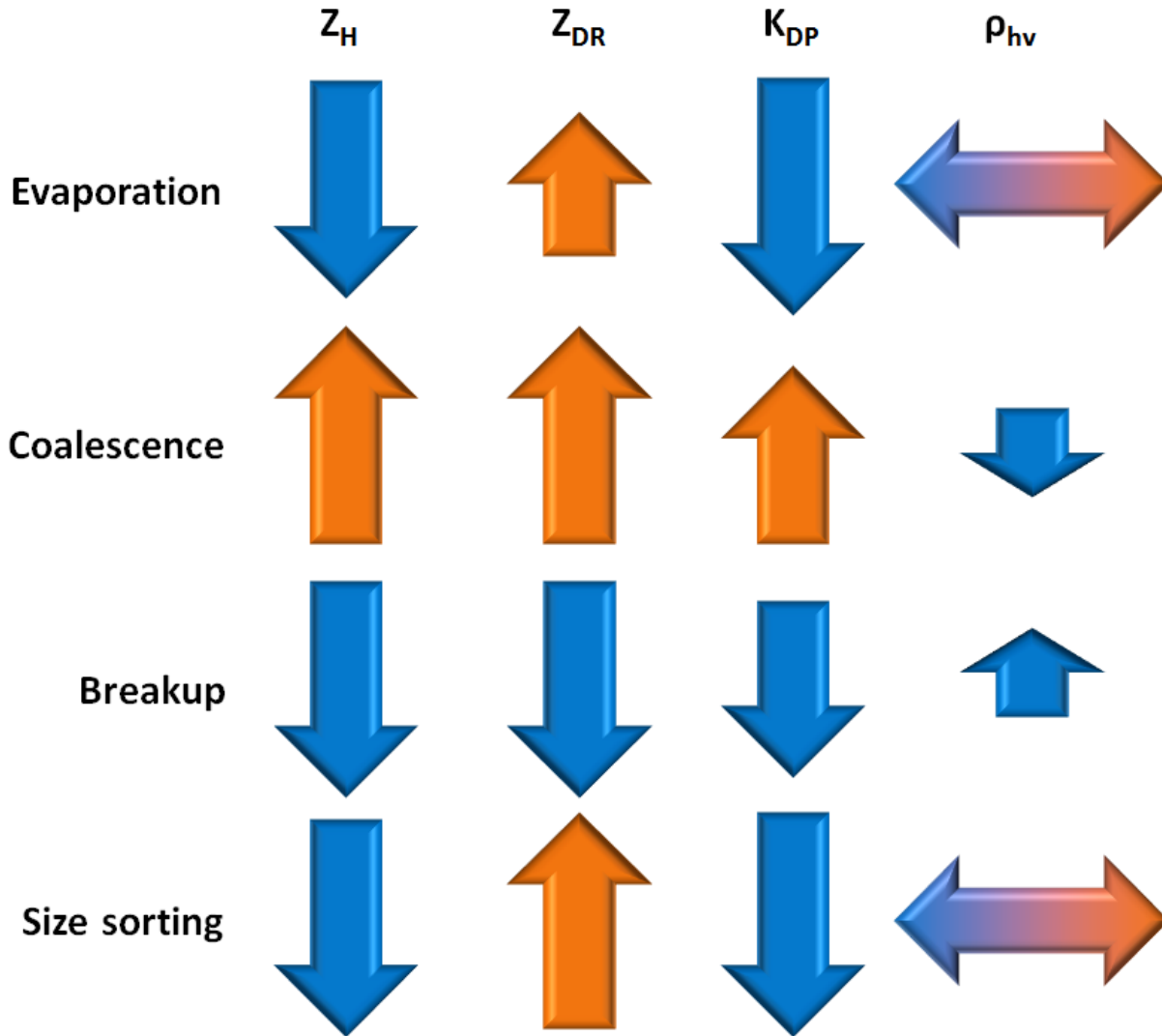


Fig. 14: Schematic summarizing the impact of the warm-rain processes on the polarimetric variables. Direction of the arrows indicates direction of change in the variable towards the ground when a process is ongoing. Double-headed arrows indicate that changes depend on other factors, such as the DSD.

the polarimetric radar variables, which are validated by the observations. Such retrievals provide experimental evidence that can be used for comparison with various models and parameterizations of the warm-rain physical processes. Additionally, they provide a basis for better understanding of how such microphysical processes affect rainfall rate beneath cloud base, which can be used to improve the accuracy of remote quantitative precipitation estimation.

### 8. Acknowledgments.

Funding was provided by NOAA/Office of Oceanic and Atmospheric Research under NOAA-University of Oklahoma Cooperative Agreement #NA11OAR4320072, U.S. Department of Commerce. Additional funding comes from the Meteorological Institute of the University of Bonn, where the first author held a Doctoral Fellowship funded by the Deutsche Forschungsgemeinschaft (DFG) as part of the Transregional Research Center on "Patterns in

Landsurface-Vegetation-Atmosphere Interactions" (TR32).

## 9. References.

Atlas, D., and C. W. Ulbrich, 1977: Path- and area-integrated rainfall measurement by microwave attenuation in the 1–3 cm band. *J. Appl. Meteor.*, **16**, 1322–1331.

Brandes, E. A., G. Zhang, and J. Vivekanandan, 2002: Experiments in rainfall estimation with a polarimetric radar in a subtropical environment. *J. Appl. Meteor.*, **41**, 674–685.

Brandes, E. A., G. Zhang, and J. Vivekanandan, 2004: Drop size distribution retrieval with polarimetric radar: Model and application. *J. Appl. Meteor.*, **43**, 461–475.

Brown, P. S., 1986: Analysis of the Low and List drop-breakup formulation. *J. Climate Appl. Meteor.*, **25**, 313–321.

Brown, P.S., 1987: Parameterization of drop-spectrum evolution due to coalescence and breakup. *J. Atmos. Sci.*, **44**, 242–249.

Brown, P.S., 1993: Analysis and parameterization of the combined coalescence, breakup, and evaporation processes. *J. Atmos. Sci.*, **50**, 2940–2951.

Brown, P.S., 1994: Vertical variation of the steady-state drop spectrum in a one-dimensional rain shaft. *J. Atmos. Sci.*, **51**, 2075–2085.

Brown, P.S., 1995: Structural stability of the coalescence/breakup equation. *J. Atmos. Sci.*, **52**, 3857–3865.

Cao, Q., G. Zhang, E. Brandes, T. Schuur, A. V. Ryzhkov, and K. Ikeda, 2008: Analysis of video disdrometer and polarimetric radar data to characterize rain microphysics in Oklahoma. *J. Appl. Meteor. Climatol.*, **47**, 2238–2255.

Gillespie, J.R., and R. List, 1978: Effects of collision-induced breakup on drop size distributions in steady-state rain-shafts. *Pure Appl. Geophys.*, **117**, 599–626.

Kumjian, M.R., and A.V. Ryzhkov, 2010: The impact of evaporation on polarimetric characteristics of rain: Theoretical model and practical implications. *J. Appl. Meteor. and Climatol.*, **49**, 1247–1267.

Kumjian, M.R., and A.V. Ryzhkov, 2012: The impact of size sorting on the polarimetric radar variables. *J. Atmos. Sci.*, **in press**.

List, R., and J.R. Gillespie, 1976: Evolution of raindrop spectra with collision-induced breakup. *J. Atmos. Sci.*, **33**, 2007–2013.

List, R., and G. M. McFarquhar, 1990: The evolution of threepk raindrop size distributions in one-dimensional shaft models. Part I: Single-pulse rain. *J. Atmos. Sci.*, **47**, 2996–3006.

List, R., N. R. Donaldson, and R. E. Stewart, 1987: Temporal evolution of drop spectra to collisional equilibrium in steady and pulsating rain. *J. Atmos. Sci.*, **44**, 362–372.

Low, T. B., and R. List, 1982a: Collision, coalescence, and breakup of raindrops. Part I: Experimentally established coalescence efficiencies and fragment size distributions in breakup. *J. Atmos. Sci.*, **39**, 1591–1606.

Low, T. B., and R. List, 1982b: Collision, coalescence, and breakup of raindrops. Part II: Parameterization of fragment size distributions. *J. Atmos. Sci.*, **39**, 1607–1618.

Mishchenko, M. I., 2000: Calculation of the amplitude matrix for a nonspherical particle in a fixed orientation. *Appl. Opt.*, **39**, 1026–1031.

Moisseev, D. N., and V. Chandrasekar, 2007: Examination of the  $\mu$ - $\Lambda$  relation suggested for

drop size distribution parameters. *J. Atmos. Oceanic Technol.*, **24**, 847–855.

Pruppacher, H. R., and J. D. Klett, 1997: *Microphysics of Clouds and Precipitation*. 2nd ed. Oxford University Press, 953 pp.

Rogers, R. R., and M. K. Yau, 1989: *A Short Course in Cloud Physics*. 3rd ed. Elsevier Press, 290 pp.

Ryzhkov, A. V., 2001: Interpretation of polarimetric radar covariance matrix for meteorological scatterers: Theoretical analysis. *J. Atmos. Oceanic Technol.*, **18**, 315–328.

Ryzhkov, A.V., M. Pinsky, A. Pokrovsky, and A. Khain, 2011: Polarimetric radar observation operator for a cloud model with spectral microphysics. *J. Appl. Meteor. and Climatol.*, **50**, 873-894.

Seifert, A., 2005: On the shape–slope relation of drop size distributions in convective rain. *J. Appl. Meteor.*, **44**, 1146–1151

Zhang, G., J. Vivekanandan, and E. Brandes, 2001: A method for estimating rain rate and drop size distribution from polarimetric radar measurements. *IEEE Trans. Geosci. Remote Sens.*, **39**, 830–841.

Zhang, G., J. Vivekanandan, E. A. Brandes, R. Meneghini, and T. Kozu, 2003: The shape–slope relation in observed gamma raindrop size distributions: Statistical error or useful information? *J. Atmos. Oceanic Technol.*, **20**, 1106–1119.